International Research Journal of Engineering and Technology (IRJET) e-ISSN: 2395-0056
Volume: 10 Special Issue: | Apr 2023 www.irjet.net p-ISSN: 2395-0072

International Conference on Recent Trends in Engineering & Technology- 2023 (ICRTET-3)
Organised by: VSM College of Engineering, Ramachandrapuram

Optimization Of Energy Utilization to Electrical Vehicle By Multi Section Control Strategy With AdaptiveNeuro Fuzzy Inference System (ANFIS)

ATTI V V SRINIVAS[1], P. SRIDEVI[2], D. SANDHYA RANI,[3]

[123] *Associate Professor, Dept. of EEE, VSM COLLEGE OF ENGINEERING, Ramachandrapuram, A.P, India*

ABSTRACT:. Switched reluctance motors (SRMs) are one of thepromised motors for EV applications. In order to extend the EVs' driving miles, the use of photovoltaic (PV) panels on the vehicle helps to decrease the dependency on vehicle batteries. Based on the phase winding characteristics of SRMs, a tri port converter with Adaptive Neuro Fuzzy Inference System (ANFIS) is proposed in this paper to control the energy flow among the PV panel, battery, and SRM. By using ANFIS, we can get low THD values and smooth waveforms. Six operating modes are presented, four of which are developed for driving and two for standstill on board charging. In the driving modes, the energy decoupling control for maximum power point tracking (MPPT) of the PV panel and speed control of the SRM are grasp. In the standstill charging modes, a grid connected charging topology is developed without a need for external hardware. When the PV panel directly charges the battery, a multisection charging control strategy is used to optimize energy utilization. Simulation results based on MATLAB/Simulink .

Index Terms—Electric vehicles (EVs), photovoltaic's (PVs), power flow control, switched reluctance motors (SRMs), tri-port converter,Adaptive Neuro Fuzzy Interface Systems(ANFIS).

I. INTRODUCTION

Electric vehicles (EVs) have taken a significant leap forward by advances in motor drives, power converters, batteries, and energy management systems [1]–[4]. However, due to the limitation of current battery technologies, the drivingmiles are relatively short that restricts the wide application of EVs [5]–[7]. In terms of motor drives, high-performance permanent-magnet (PM) machines are widely used while rare-earth materials are needed in large quantities, limiting the wide application of EVs [8], [9].In order to overcome these issues, a photovoltaic (PV) panel and a switched reluctance motor (SRM) are introduced to pro-vide power supply and motor drive, respectively. First, by adding the PV panel on top of the EV, a sustainable energy source is achieved. Nowadays, a typical passenger car has a surface enough to install a 250-W PV panel [10]. Second, a SRM needs no rare- earth PMs and is also robust so that it receives increasing attention in EV applications [11]–[16]. While PV panels have low-power density for traction drives, they can be used to charge batteries most of time.

Generally, the PV-fed EV has a similar structure to the hybrid electrical vehicle (HEV), whose internal combustion engine (ICE) is replaced by the PV panel. The PV-fed EV system is illustrated in Fig. 1. Its key components include an off-board charging station, a PV, batteries, and power converters [17] – [19]. In order to decrease the energy conversion processes, one approach is to redesign the motor to include some onboard charging functions [20]–[22]. For instance, paper [22] designs a 20-kW split- phase PM motor for EV charging, but it suffers from high harmonic contents in the back electromotive force (EMF). Another solution is based on a traditional SRM. Paper [23] achieves onboard charging and power factor correction in a 2.3-kW SRM by employing machine windings as the input filter inductor. The concept of modular structure of driving topology is proposed in paper [24]. Based on the intelligent power modules (IPMs), a four- phase half bridge converter is employed to achieve driving and grid-charging. Although modularization supports mass production, the use of half/full bridge topology reduces the system reliability (e.g., shoot-through issues). Paper [25] develops a simple topology for plug-in HEV that supports flexible energy flow. But for grid-charging, the grid should be connected to the generator rectifier that increases the energy conversion process and decreases the charging efficiency. Nonetheless, an effective topology and control strategy for PV-fed EVs is not yet developed. Because the PV has different characteristics to ICEs, MPPT and solar energy utilization are the unique factors for the PV-fed EVs.

In order to achieve low-cost and flexible energy flow modes, a low-cost tri-port converter is proposed in this paper to coordinate the PV panel, SRM, and battery. Six operational modes are developed to support flexible control of energy flow.

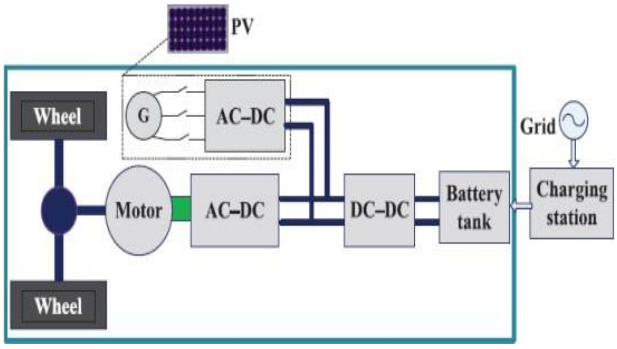

Fig. 1.PV-fed HEV.

II. TOPOLOGY AND OPERATIONAL MODES

A. Proposed Topology and Working Modes

The proposed tri-port topology has three energy terminals, PV, battery, and SRM. They are linked by a power converter that consists of four switching devices (S_0–S_3), four diodes (D_0–D_3), and two relays, as shown in Fig. 2 [26].

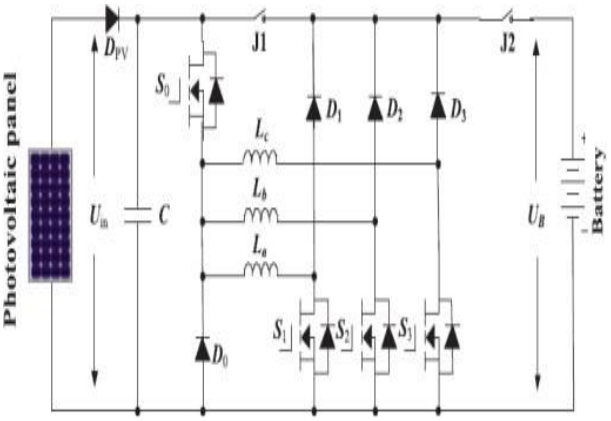

Fig. 2.Proposed tri-port topology for PV-powered SRM drive.

By controlling relays J1 and J2, the six operation modes are supported, as shown in Fig. 3; the corresponding relay actions are illustrated in Table I. In mode 1, PV is the energy source to drive the SRM and to charge the battery. In mode 2, the PV and battery are both the energy sources to drive the SRM. In mode 3, the PV is the source and the battery is idle. In mode 4, the battery is the driving source and the PV is idle. In mode 5, thebattery is charged by a single-phase grid while both the PV and SRM are idle. In mode 6, the battery is charged by the PV and the SRM is idle.

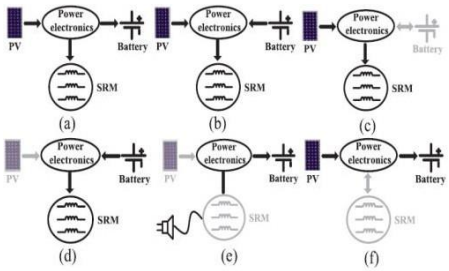

Fig. 3.Six operation modes of the proposed tri-port topology. (a) Mode 1.(b) Mode 2. (c) Mode 3. (d) Mode 4. (e) Mode 5. (f) Mode 6.

TABLE I
J1 AND J2 ACTIONS UNDER DIFFERENT MODES

Mode	J1 and J2
1	J1 turn-off; J2 turn-on
2	J1 and J2 turn-on
3	J1 turn-on; J2 turn-off
4	J1 and J2 turn-on
5	J1 and J2 turn-on
6	J1 turn-off; J2 turn-on

B. Driving Modes

Operating modes 1–4 are the driving modes to provide tractiondrive to the vehicle.

1) Mode 1: At light loads of operation, the energy generated from the PV is more than the SRM needed; the system operates in mode 1. The corresponding operation circuitis shown in Fig. 4(a), in which relay J1 turns off and relay J2 turns on. The PV panel energy feeds the energy to SRM and charges the battery; so in this mode, the battery is charged in EV operation condition.

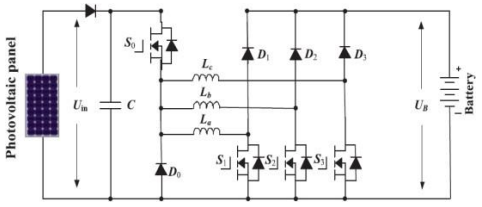

(a) Operation circuit under mode 1

2) Mode 2: When the SRM operates in heavy load such as uphill driving or acceleration, both the PV panel and battery supply power to the SRM. The corresponding operation circuit is shown in Fig. 4(b), in which relay J1 and J2 are turned on.

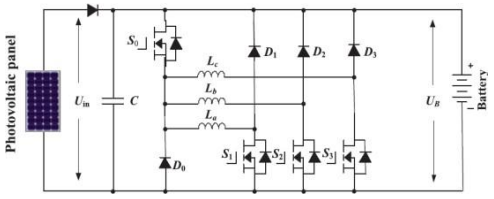

(a) Operation circuit under mode 2

3) Mode 3: When the battery is out of power, the PVpanel is the only energy source to drive the vehicle. Thecorresponding circuit is shown in Fig. 4(c). J1 turns on and J2 turns off.

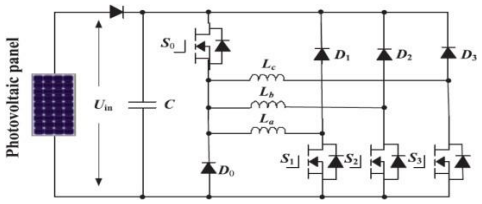

(c) Operation circuit under mode3.

4) Mode 4: When the PV cannot generate electricity due to lowsolar irradiation, the battery supplies power to the SRM. The corresponding topology is illustrated in Fig. 4(d). In this mode, relay J1 and J2 are both conducting.

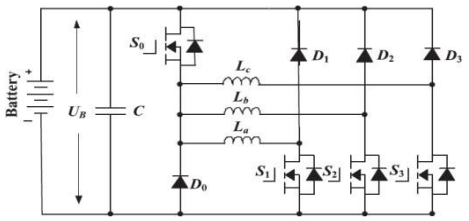

(d) Operation circuit under mode 4

C. Battery Charging Modes

Operating modes 5 and 6 are the battery charging modes.

5) Mode 5: When PV cannot generate electricity; an external power source is needed to charge the battery, such as ac grid. The corresponding circuit is shown in Fig. 5(a). J1 and J2 turn on. Point A is central tapped of phase windings that can be easily achieved without changing the motor structure. One of the three-phase windings is split and its midpoint is pulled out, as shown in Fig. 5(a). Phase windings La1 and La2 are employed as input filter inductors. These inductors are part of the drive circuit to form an ac–dc rectifier for grid-charging.

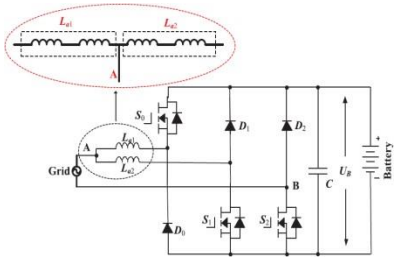

(a) Grid charging mode

6) Mode 6: When the EV is parked under the sun, thePV can charge the battery. J1 turns off and J2 turns on.

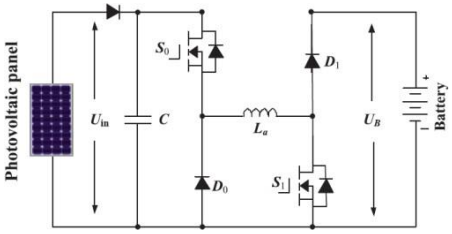

(b) PV source charging mode.

III. CONTROL STRATEGY UNDER DIFFERENT MODES

In order to make the best use of solar energy for driving theEV, a control strategy under different modes is designed.

A. Single Source Driving Mode

According to the difference in the power sources, there are PV-driving, battery-driving, and PV and battery parallel fed source. In a heavy load condition, the PV power cannot support the EV, mode 2 can be adopted to support enough energy and make full use of solar energy. Fig. 6(a) shows the equivalent power source; the corresponding PV panel working pointsare illustrated in Fig. 6(b). Because the PV is paralleled with the battery, the PV panel voltage is clamped to the battery voltage U_B. In mode 2, there are three working states: winding excitation, energy recycling, and freewheeling states, as shown in Fig. 7. Modes 3 and 4 have similar working states to mode 2. The difference is that the PV is the only source in mode 3 while the battery is the only source in mode 4.

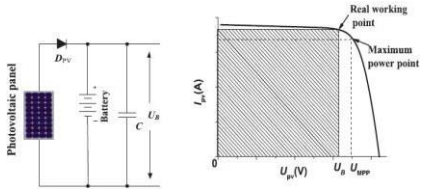

(a) (b)

Fig. 6.Power supply at mode 2. (a) Compound power source.

(b) Workingpoint of the PV.

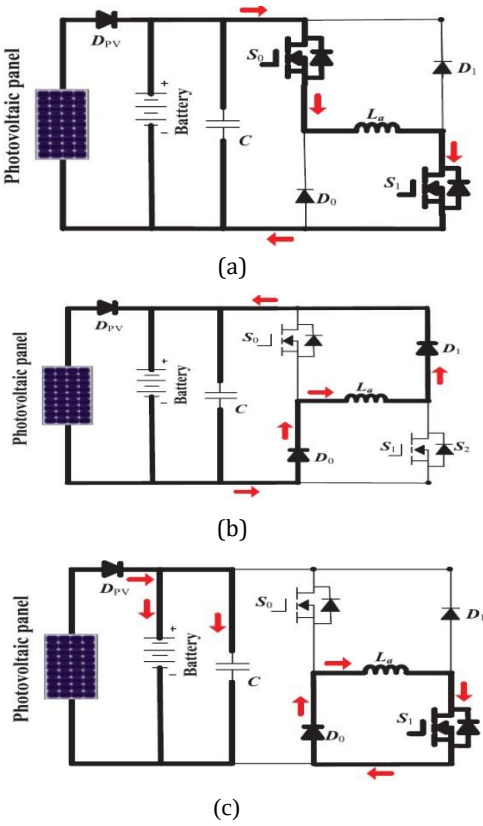

Fig. 7. Working states at mode 2. (a) Winding excitation state. (b) Energy recycling state. (c) Freewheeling state.

Neglecting the voltage drop across the power switches and diodes, the phase voltage is given by

$$U_{\text{in}} = R_k i_k + \frac{d\psi(i_k, \theta_r)}{dt} = R_k i_k + L_k \frac{di_k}{dt} + i_k \omega_r \frac{dL_k}{d\theta_r}, \quad k = a, b, c \qquad (1)$$

where U_{in} is the dc-link voltage, k is phases a, b, or c,R_k is the phase resistance, i_k is the phase current, L_k is the phase inductance, ϑ_r is the rotor position, $\psi(i_k, \vartheta_r)$ is the phase flux linkage depending on the phase current and rotor position, and $\omega_r$is the angular speed.

The third term in (1) is the back EMF voltage given by

$$e_k = i_k \omega_r \frac{dL_k}{d\theta_r}. \qquad (2)$$

Hence, the phase voltage is found by

$$U_k = R_k i_k + L_k \frac{di_k}{dt} + e_k. \qquad (3)$$

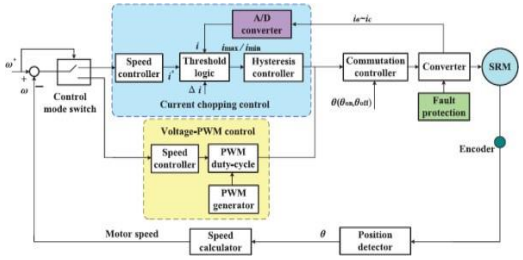

Fig. 8. SRM control strategy under single-source driving mode.

In the excitation region, turning on S_0 and S_1 will induce a current in phase a winding, as shown in Fig. 7(a). Phase a winding is subjected to the positive dc bus voltage

$$+U_{\text{in}} = R_k i_k + L_k \frac{di_k}{dt} + e_k. \qquad (4)$$

When S_0 is OFF and S_1 is ON, the phase current is in a free-wheeling state in a zero-voltage loop, as shown in Fig. 7(c), thephase voltage is zero

$$0 = R_k i_k + L_k \frac{di_k}{dt} + e_k. \qquad (5)$$

In the demagnetization region, S_0 and S_1 are both turned off, and the phase current will flow back to the power supply, as shown in Fig. 7(b). In this state, the phase winding issubjected to the negative dc bus voltage, and the phase voltage is

$$-U_{\text{in}} = R_k i_k + L_k \frac{di_k}{dt} + e_k. \qquad (6)$$

In single-source driving mode, the voltage-PWM control is employed as the basic scheme, as illustrated in Fig. 8. According to the given speed ω^*, the voltage-PWM control is activated at speed control.

B. Driving-Charging Hybrid Control Strategy

In the driving-charging hybrid control, the PV is the driving source and the battery is charged by the freewheeling current, as illustrated in drive mode 1. There are two control objectives: MPPT of the PV panel and speed control of the SRM.The dual-source condition is switched from a PV-driving mode. First, the motor speed is controlled at a given speed in mode 3. Then, J2 is turned on and J1 is turned off to switch to mode 1. By controlling the turn-off angle, the maximum power of PV panel can be tracked.There are three steady working states for the dual-source mode (mode 1), as shown in Fig. 9. In Fig. 9(a), S_0 and S_1 con-duct, the PV panel charges the SRM

winding to drive the motor. In Fig. 9(b), S_0 and S_1 turn-off; and the battery is charged with freewheeling current of the phase winding. Fig. 9(c) shows a freewheeling state.

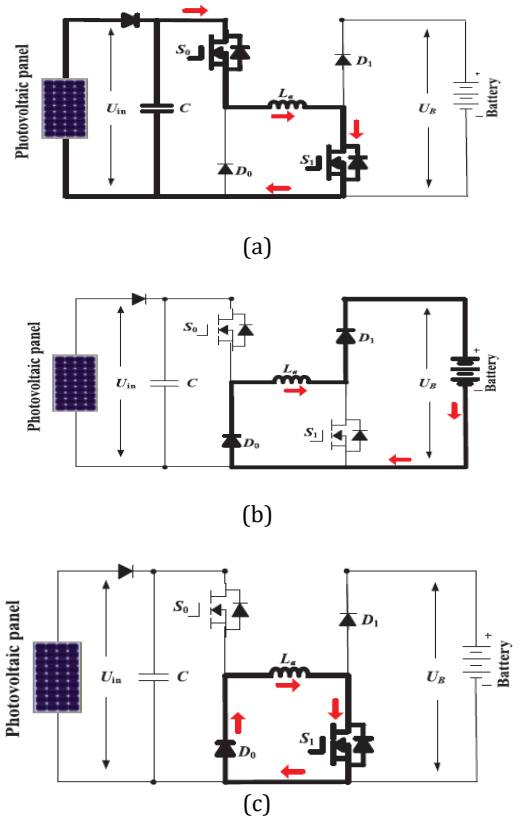

Fig. 9.Mode 1 working states. (a)Winding exciting state. (b)Battery chargingstate. (c) Freewheeling state.

Fig. 10 is the control strategy under driving-charging mode. In Fig. 10, ϑ_{on} is the turn-on angle of SRM; ϑ_{off} is the turn off angle of SRM. By adjusting turn-on angle, the speed of SRMcan be controlled; the MPPT of PV panel can be achieved by adjusting turn off angle, which can control the charging current to the battery.Can be controlled; the MPPT of PV panel can be achieved by adjusting turn-off angle, which can control the charging current to the battery.

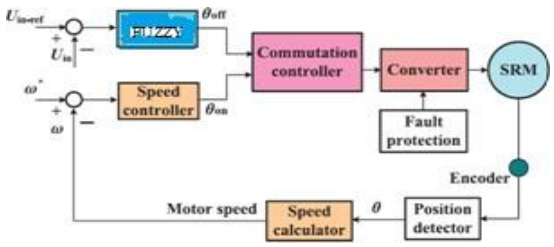

Fig. 10. Control strategy under driving charging mode (mode1).

C. Grid-Charging Control Strategy

The proposed topology also supports the single-phase grid-charging. There are four basic charging states and S_0 is always turned off. When the grid instantaneous voltage is over zero, the two working states are presented in Fig. 11(a) and (b).In Fig. 11(a), S_1 and S_2 conduct, the grid voltage charges the phase winding L_{a2}, the corresponding equation can be expressed as (7); in Fig. 11(b), S_1 turns off and S_2 conducts, the grid is connected in series with phase winding to charges the battery, the corresponding equation can be expressed as (8)

$$U_{\text{grid}} = L_{a2} \cdot \frac{di_{\text{grid}}}{dt} \quad (7)$$

$$U_B - U_{\text{grid}} = L_{a2} \cdot \frac{di_{\text{grid}}}{dt}. \quad (8)$$

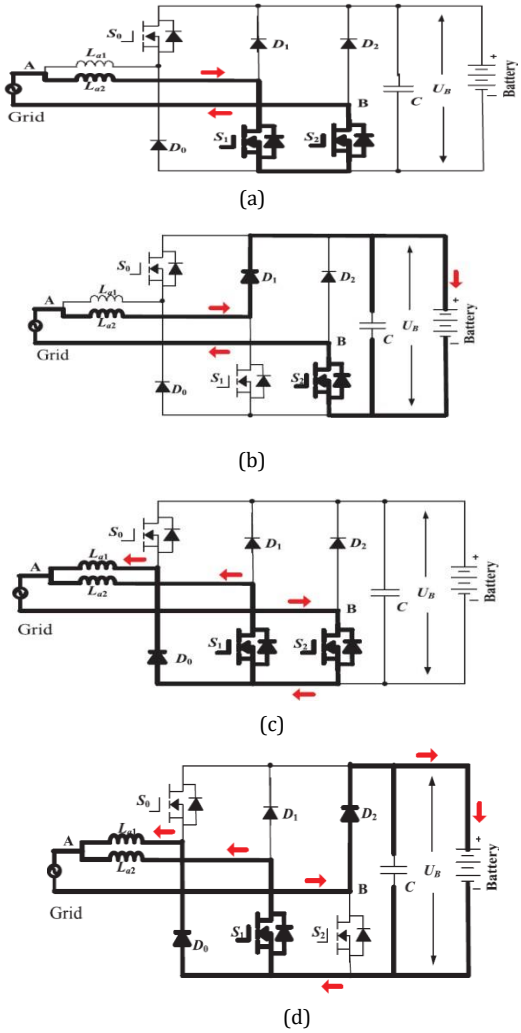

Fig. 11.Mode 5 charging states. (a) Grid charging state 1(Ugrid>0). (b) Gridcharging state 2 (Ugrid>0). (c) Grid charging state 3 (Ugrid<0). (d) Gridcharging state 4 (Ugrid<0).

When the grid instantaneous voltage is below zero, the two working states are presented in Fig. 11(c) and (d). In Fig. 11(c), $S_1$and S_2conduct, the grid voltage charges the phase wind-ingL_{a1} and L_{a2}, the corresponding equation can be expressed as (9); in Fig. 11(d), S_1 keeps conducing and S_2 turns off, the grid is connected in series with phase winding L_{a1} and $L_{a2}$to charges the battery, the corresponding equation can beexpressed as (10)

$$U_{\text{grid}} = \frac{L_{a1} + L_{a2}}{L_{a1} \cdot L_{a2}} \cdot \frac{di_{\text{grid}}}{dt} \quad (9)$$

$$-U_B - U_{\text{grid}} = \frac{L_{a1} + L_{a2}}{L_{a1} \cdot L_{a2}} \cdot \frac{di_{\text{grid}}}{dt}. \quad (10)$$

In Fig. 12, U_{grid} is the grid voltage; by the phase lock loop (PLL), the phase information can be got; $I_{\text{ref\_grid}}$ is thegiven amplitude of the grid current. Combining sin ϑ and$I_{\text{ref_grid}}$, the instantaneous grid current reference$i_{\text{ref_grid}}$canbe calculated. In this mode, when U_{grid}> 0, the inductance is L_{a2}; when U_{grid}< 0, the inductance is paralleled L_{a1} and L_{a2}; in order to adopt the change in the inductance, hysteresis control is employed to realize grid current regulation. Furthermore, hysteresis control has excellent loop performance, global stability, and small phase lag that make grid-connected control stable.

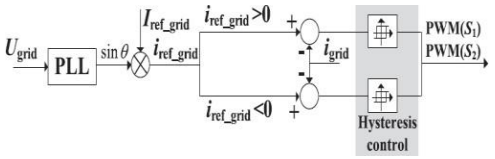

Fig. 12.Grid-connected charging control (mode 5).

TABLE II

SIMULATION PARAMETERS

Parameter	Value
SRM	6/4
PV panel Maximum power point voltage reference voltage	310 V
Battery voltage	350 V
Constant voltage control reference voltage	355 V
Constant current control reference current	1 A
Mode 1, charging current	60 A
Mode 4, driving speed	1250 r/min
Mode 6, constant voltage charging reference	355 V
Mode 6, constant current charging reference	1 A

D. PV-Fed Charging Control Strategy

In this mode, the PV panel charges the battery directly by the driving topology. The phase windings are employed as inductor, and the driving topology can be functioned as interleaved buck– boost charging topology. For one phase, there are two states, as shown in Fig. 13(a) and (b). When S_0 and S_1 turn on, the PV panel charges phase inductance; when S_0 and S_1 turn off, the phase inductance discharges energy to battery. According to the state-of- charging (SoC), there are three stages to make full use of solar energy and maintain battery healthy condition, as illustrated in Fig. 13(c). During stage 1, the corresponding battery SoC is in SoC0 – SoC1, the battery is in extremely lack energy condition, the MPPT control strategy is employed to make full use of solar energy. During stage 2, the corresponding battery SoC is in SoC1 – SoC2, the constant-voltage control is adopted to charge the battery. During stage 3, the corresponding battery SoC is in SoC2 – 100%, the micro- current charging is adopted. In order to simplify the control strategy, constant voltage is employed in PV panel MPPT control.

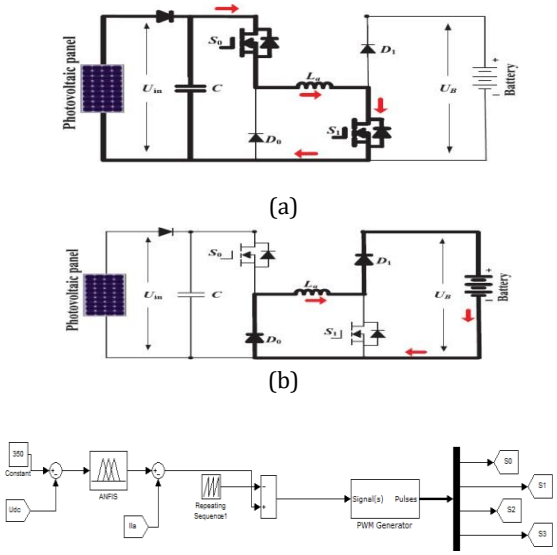

Fig. 13. Mode 6 charging states and control strategy. (a) Phase inductance charging. (b) Battery charging. (c) Simulink model of the ANFIS Controller.

DESIGN OF ADAPTIVE NEURO-FUZZY CONTROLLER

Adaptive Neuro fuzzy inference system (ANFIS) integrates the best features of fuzzy systems and neural networks, and it has potential to capture the benefits of both in a single frame work. ANFIS is a kind of artificial neural network that is based on Takagi-Sugeno fuzzy inference system, which is having one input an done output. Using a given data set, the toolbox function of ANFIS constructs a fuzzy inference system (FIS) where as the membership function parameters are tuned (adjusted) using a back propagation algorithm. In order to have an idea of optimized ANFIS architecture for proposed control, an initial data is generated from normal *PI* regulator and the data is saved in workspace of MATLAB. Then the ANFIS command windowis opened by typing anfiseditorin the main MATLAB window. Then the data previously saved in workspace is loaded in the ANFIS command window to generate an optimized ANFISarchitecture as shown in Fig.14.

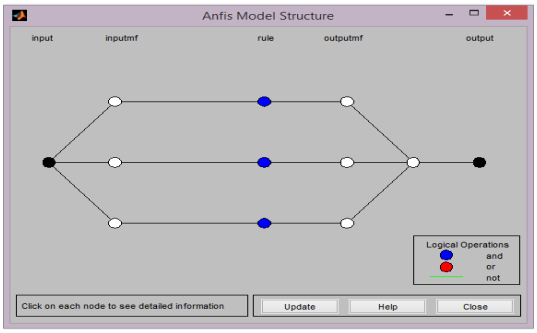

Fig.14:Optimized ANFIS architecture suggested byMATLAB/ANFISeditor.

In Fig.15 shows schematic of the proposed ANFIS based control architecture. The node functions of each layer in the ANFIS architecture are described as follows:

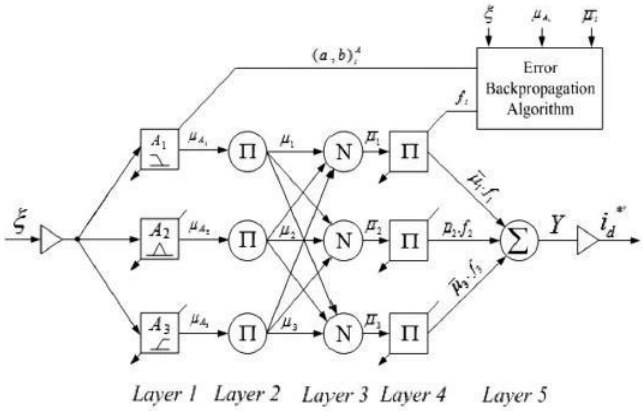

Fig. 15: Schematic of the proposed ANFIS-based control architecture.

The error between reference dc-link voltage and actual dc-link voltage ($\xi=V_{dc}^*-V_{dc}$) is given to the Neuro-fuzzy controller and the same error is used to tune the precondition and consequent parameters [10]. The control of dc-link voltage gives the active power current component (i_d *'), which is further modified to take in account of active current component injected from RES (i_{Ren}).The node functions of each layer in ANFIS architecture are as described below:

Layer 1: This layer is also known as fuzzification layer where each node is represented by square. Here, three membership functions are assigned to each input. The trapezoidal and triangular membership functions are used to reduce the computation burden as shown in Fig. 16. And the corresponding node equations are as given below:

$$\mu_{A1}(\varepsilon) = \begin{cases} 1 & \varepsilon \le b_1 \\ \dfrac{\varepsilon - a_1}{b_1 - a_1} & b_1 < \varepsilon < a_1 \\ 0 & \varepsilon \ge a_1 \end{cases} \mu_{A2}(\varepsilon) = \left\{1 - \frac{\varepsilon - a_1}{0.5b_2} \quad |\varepsilon - a_2| \le 0.5b_2 \right\}^2$$

$$\mu_{A3}(\varepsilon) = \begin{cases} 0 & \varepsilon \le a_3 \\ \dfrac{\varepsilon - a_1}{b_1 - a_1} & a_3 < \varepsilon < b_3 \\ 1 & \varepsilon \ge b_3 \end{cases} \qquad (12)$$

Where the value of parameters (a_i, b_i) changes with the change in error and accordingly generates the linguistic value of each membership function. Parameters in this layer are referred as premise parameters or precondition parameters.

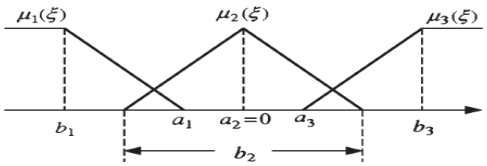

Fig. 16: Fuzzy membership functions.

Layer 2: Every node in this layer is a circle labelled as Π. which multiplies the incoming signals and forwards it to next layer

$\mu_i = \mu_A(\varepsilon_1).\ \mu_{Bi}\ (\varepsilon_2)$ … … i=1,2,3,...But in our case there is only one input, so this layer can be ignored and the output of first layer will directly pass to the third layer. Here, the output of each node represents the firing strength of a rule.

Layer 3: Every node in this layer is represented as circle. This layer calculates the normalized firing strength of each rule as given below:

$$\bar{\mu}_i = \frac{\mu_i}{1+\mu_2+\mu_3} \quad (13)$$

Layer 4: Every node in this layer is a node function

$$O_i = \bar{\mu}_i . f_i = \bar{\mu}_i (a_0^i + a_1^i \varepsilon) \quad i=1,2,3.$$

where the parameters (a_0^i, a_1^i) are tuned as the function of input (ξ). The parameters inthis layer are also referred as consequentparameters.

Layer 5: This layer is also called output layer which computesthe output

IV. MATLAB /SIMULINK results

A 6/4 SRM is first modeled in MATLAB/Simulink using parameters in Table II. Fig. 18(a) presents the simulation results at mode 1. The load torque is set as 35 Nm; the PV panel voltage is controlled at the MPP. The freewheeling current is used to charge the battery. Fig. 18(b) shows the simulation results of the single-source driving modes (modes 2–4).

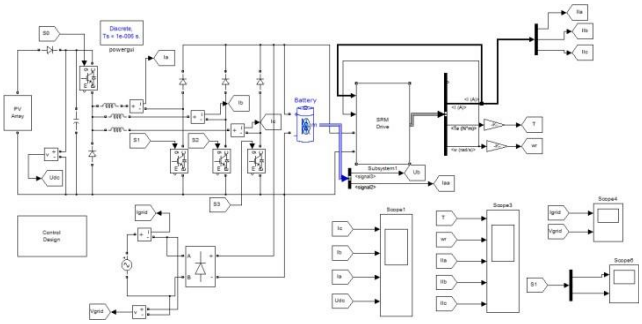

Fig 17 MATLAB SIMULINK Model of the proposed PV fed HV's using ANFIS Logic Controller.

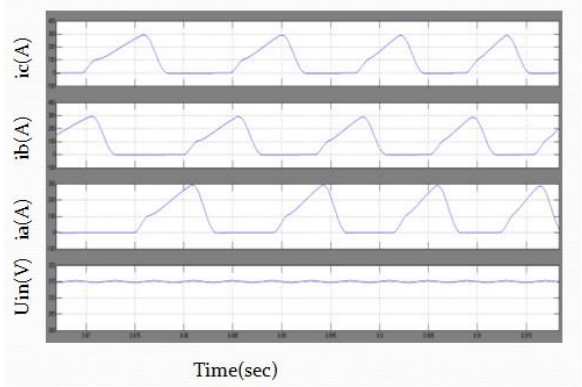

(a)

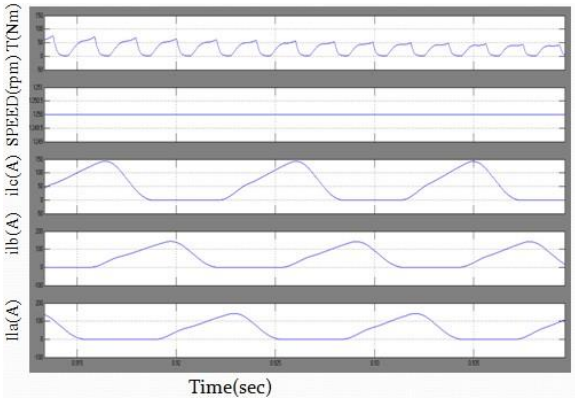

(b)

Fig. 18. Simulation results for driving conditions at modes 1, 3,and 4.(a) Simulation results of driving-charging mode (mode 1). (b) Simulation results of single-source driving mode (modes3 and 4).

Fig. 19 shows the simulation results of charging where Fig. 19(a) is for grid-charging. The positive half current quality is better than the negative half that is caused by the change in the grid-connected inductance.

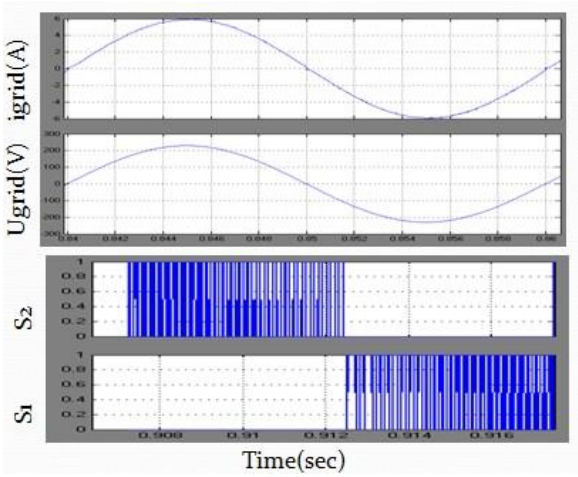

(a)

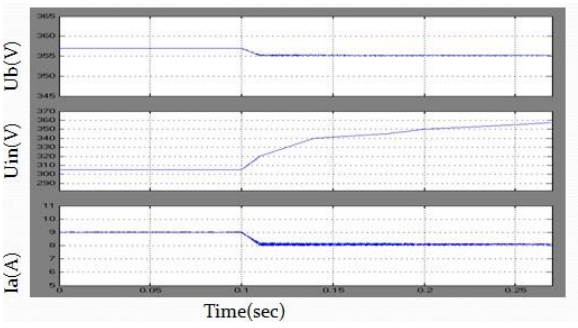

(b)

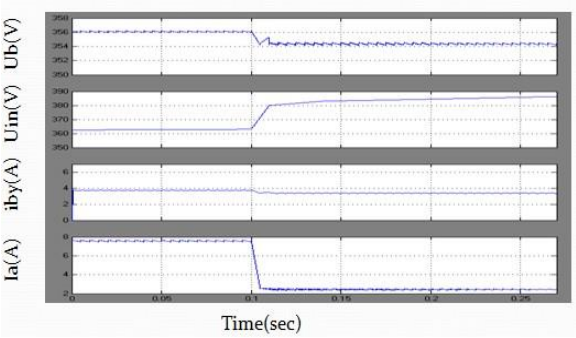

(c)

Fig. 19. Simulation results for charging modes. (a) Grid charging (mode 5).(b) PV charging mode 6 (stages 1–2). (c)PV charging mode 6 (stages 2–3).

Fig. 19(b) and (c) is for PV-charging. Fig. 19(b) presents the step change from stage 1 to 2. In stage 1, the battery is low in SoC. In order to achieve MPPT of the PV, the constant-voltage control is employed and the PV output voltageis controlled at MPP (310 V), as shown in Fig. 15(b). In stage 2, a constant-voltage is adopted; the reference voltage is set to 355 V. As shown in Fig. 19(b), the charging converter output voltage is controlled at reference voltage in the step change from stage 1 to 2. In stage 3, 1-A trickle charging is also achieved, as shown in Fig. 19(c).

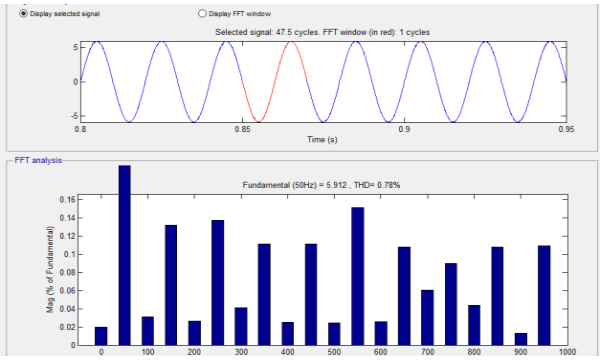

Fig20 THD value of the input current in %

CONCLUSION

In order to tackle the range anxiety of using EVs and decrease the system cost, a combination of the PV panel and SRM with ANFIS Controller is proposed as the EV driving system.The main contributions of this paper are as follows.A tri-port converter is used to coordinate the PV panel, battery, and SRM.Six working modes are developed to achieve flexible energy flow for driving control, driving/charging hybrid control, and charging control.A novel grid-charging topology is formed without a need for external power electronics devices.A PV-fed battery charging control scheme is developed toimprove the solar energy utilization.Since PV-fed EVs are a greener and more sustainable technology than conventional ICE vehicles, this work will provide a feasible solution toreduce the total costs and CO_2 emissions of electrified vehicles. Furthermore, the proposed technology may also be applied to similar applications such as fuel cell powered EVs. Fuel cells have a much high-power density and are thus better suited for EV applications.

REFERENCES

[1] A. Emadi, L. Young-Joo, and K. Rajashekara, "Power electronics and motor drives in electric, hybrid electric, and plug-in hybrid electric vehicles," *IEEE Trans. Ind. Electron.*, vol. 55, no. 6, pp. 2237–2245, Jun. 2008.

[2] L. K. Bose, "Global energy scenario and impact of power electronics in 21st century," *IEEE Trans. Ind. Electron.*, vol. 60, no. 7, pp. 2638–2651, Jul. 2013.

[3] J. De Santiago *et al.*, "Electrical motor drivelines in commercial all-electric vehicles: A review," *IEEE Trans. Veh. Technol.*, vol. 61, no. 2, pp. 475–484, Feb. 2012.

[4] Z. Amjadi and S. S. Williamson, "Power-electronics- based solutions for plug-in hybrid electric vehicle energy storage and management systems," *IEEE Trans. Ind. Electron.*,vol. 57, no. 2, pp. 608–616, Feb. 2010.

[5] A. Kuperman, U. Levy, J. Goren, A. Zafransky, and A. Savernin, "Battery charger for electric vehicle traction battery switch station," *IEEE Trans.Ind. Electron.*, vol. 60, no. 12, pp. 5391–5399, Dec. 2013.

[6] S. G. Li, S. M. Sharkh, F. C. Walsh, and C. N.Zhang, "Energy and battery management of a plug-in series hybrid electric vehicle using fuzzy logic," *IEEE Trans. Veh. Technol.*, vol. 60, no. 8, pp. 3571–3585, Oct. 2011.

[7] H. Kim, M. Y. Kim, and G. W. Moon, "Amodularized charge equal-izer using a battery monitoring IC for series-connected Li-ion battery strings in electric vehicles," *IEEE Trans. Power Electron.*, vol. 28, no. 8, pp. 3779–3787, May 2013.

[8] Z. Ping, Z. Jing, L. Ranran, T. Chengde, and W. Qian, "Magnetic characteristics investigation of an axial–axial flux compound-structure PMSM used for HEVs," *IEEE Trans. Magn.*, vol. 46, no. 6, pp. 2191–2194, Jun. 2010.

[9] A. Kolli, O. Béthoux, A. De Bernardinis, E. Labouré, and G. Coquery, "Space-vector PWM control synthesis for an H-bridge drive in electric vehicles," *IEEE Trans. Veh. Technol.*, vol. 62, no. 6, pp. 2441–2452, Jul. 2013.

[10] Y. Hu, C. Gan, W. Cao, W. Li, and S. Finney, "Central-tapped node linked modular fault tolerance topology for SRM based EV/HEV applications," IEEE Trans. Power Electron., vol. 31, no. 2, pp. 1541–1554, Feb. 2016.

[11] S. M. Yang and J. Y. Chen, "Controlled dynamic braking for switched reluctance motor drives with a rectifier front end," *IEEE Trans. Ind.Electron.*, vol. 60, no. 11, pp. 4913–4919, Nov. 2013.

[12] B. Bilgin, A. Emadi, and M. Krishnamurthy, "Comprehensive evaluation of the dynamic performance of a 6/10 SRM for traction application in PHEVs," *IEEE Trans. Ind. Electron.*, vol. 60, no. 7, pp. 2564–2575, Jul. 2013.

[13] M. Takeno, A. Chiba, N. Hoshi, S. Ogasawara, M. Takemoto, and M. A. Rahman, "Test results and torque improvement of the 50-kW switched reluctance motor designed for hybrid electric vehicles," *IEEETrans. Ind. Appl.*, vol. 48, no. 4, pp. 1327–1334, Jul./Aug. 2012.

[14] A. Chiba, M. Takeno, N. Hoshi, M. Takemoto, S. Ogasawara, and M. A. Rahman, "Consideration of number of series turns in switched-reluctance traction motor competitive to HEV IPMSM," *IEEE Trans. Ind.Appl.*, vol. 48, no. 6, pp. 2333–2340, Nov./Dec. 2012.

[15] I. Boldea, L. N. Tutelea, L. Parsa, and D. Dorrell, "Automotive electric propulsion systems with reduced or no permanent magnets: An overview," *IEEE Trans. Ind. Electron.*,vol. 60, no. 9, pp. 5696–5710, Oct. 2014.

[16] X. D. Xue, K. W. E. Cheng, T. W. Ng, and N. C. Cheung, "Multi-objective optimization design of in-wheel switched reluctance motors in electric vehicles," *IEEE Trans. Ind. Electron.*, vol. 57, no. 9, pp. 2980–2987, Sep. 2010.

[17] Y. J. Lee, A. Khaligh, and A. Emadi, "Advanced integrated bidirectional AC/DC and DC/DC converter for plug-in hybrid electric vehicles," *IEEETrans. Veh. Technol.*, vol. 58,no. 8, pp. 3970–3980, Oct. 2009.

[18] M. Yilmaz and P. T. Krein, "Review of battery charger topologies, charging power levels, and infrastructure for plug-in electric and hybrid vehicles," *IEEE Trans. Power Electron.*, vol. 28, no. 5, pp. 2151–2169, May 2013.

[19] A. Khaligh and S. Dusmez, "Comprehensive topological analysis of conductive and inductive charging solutions for plug-in electric vehicles," *IEEE Trans. Veh. Technol.*, vol. 61, no. 8, pp. 3475–3489, Oct. 2012.

[20] S. Haghbin, S. Lundmark, M. Alakula, and O. Carlson, "Grid-connected integrated battery chargers in vehicleapplications: Review and new solution," *IEEE Trans. Ind. Electron.*, vol. 60, no. 2, pp. 459–473, Feb. 2013.

[21] S. Haghbin, S. Lundmark, M. Alakula, and O. Carlson, "An isolated high power integrated charger in electrified-vehicle applications," *IEEE Trans.Veh. Technol.*, vol. 60, no. 9, pp. 4115–4126, Nov. 2011.

[22] S. Haghbin, K. Khan, S. Zhao, M. Alakula, S. Lundmark, and O. Carlson, "An integrated 20-kW motor drive and isolated battery charger for plug-in vehicles," *IEEE Trans. Power Electron.*, vol. 28, no. 8, pp. 4013–4029, Aug. 2013.

[23] H. C. Chang and C. M. Liaw, "Development of a compact switched-reluctance motor drive for EV propulsion with voltage-boosting and PFC charging capabilities," *IEEE Trans. Veh. Technol.*, vol. 58, no. 7, pp. 3198–3215, Sep. 2009.

[24] H. C. Chang and C. M. Liaw, "An integrated driving/charging switched reluctance motor drive using three- phase power module," *IEEE Trans.Ind. Electron.*, vol. 58, no.5, pp. 1763–1775, May 2011.

[25] Y. Hu, X. Song, W. Cao, and B. Ji, "New SR drive with integrated charging capacity for plug-in hybrid electric vehicles (PHEVs)," *IEEE Trans.Ind. Electron.*, vol. 61, no. 10, pp. 5722–5731. Oct. 2014.

[26] Y. Hu, C. Gan, W. Cao, and S. Finney, "Tri-port converter for flexible energy control of PV-fed electric vehicles," in *Proc. IEEE Int. Elect.Mach. Drives Conf. (IEMDC'15)*, Coeur d'Alene, ID, USA, May 10–13,2015, pp. 1063–1070.